

# Dynamic Modeling of Hermetic Reciprocating Compressors, Combining Multibody Dynamics, Finite Elements Method and Fluid Film Lubrication

Edgar A. Estupiñan and Ilmar F. Santos

**Abstract**—A multibody dynamic model of the main mechanical components of a hermetic reciprocating compressor is presented in this work. The dynamics of the mechanical components are described with help of Dynamics of Multibody Systems (rigid components) and Finite Element Method (flexible components). Some of the mechanical elements are supported by fluid film bearings where the hydrodynamics interaction forces are described by the modified Reynolds equation. The system of nonlinear equations is numerically solved, taking into account the lateral and tilting vibration of the center of the crank. Particularly, in this study the main focus is on the lubrication behavior of the upper and lower bearings of the crankshaft, considering hydrodynamic lubrication conditions. The behavior of the orbits and the pressure distribution in the journal bearings is presented giving some insights into design parameters, such as, maximal fluid film pressure, minimum fluid film thickness and maximum vibration levels.

**Keywords**— Multibody dynamics, hydrodynamic lubrication, journal bearings, hermetic compressor.

## I. INTRODUCTION

Small-scale hermetic reciprocating compressors are widely used to compress coolant gas in household refrigerators and air-conditioners. Almost since the 60's these small machines became a necessary appliance in every household in the industrialized countries. Since then, a lot of research has been done to optimize the design and to improve the thermal and mechanical efficiency. Hermetic reciprocating compressors use pistons that are driven directly through a slider-crank mechanism, converting the rotating movement of the rotor to an oscillating motion. In this type of compressors, motor and compressor are directly coupled on the same shaft and the assembly is installed inside a welded steel shell. A

schematic view of a hermetic reciprocating compressor used in household refrigerators is shown in Fig. 1.

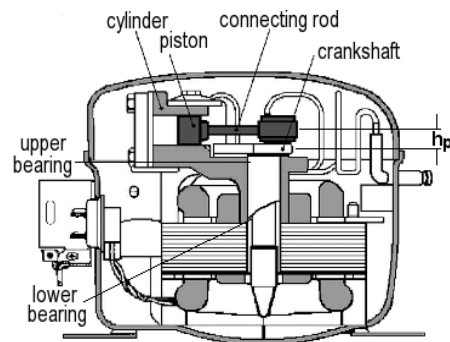


Fig. 1. Hermetic reciprocating compressor

The study and optimization of the dynamic behavior of reciprocating compressors, taking in account the hydrodynamics of bearings is of significant importance for the development of new prototypes. The performance of the bearings affects key functions such as durability, noise and vibration of the compressor. Optimization of the behavior of journal bearings by means of numerical simulation may reduce development costs for prototype testing work significantly.

Several computational models for the analysis of small reciprocating compressors can be found in the literature. They range from simple simulations including steady-state energy balance until more complex models of unsteady analysis of the heat and work transfer and thermal and fluid dynamic analysis. A complete literature review of previous studies with focus on compressor simulation models is included in [1]. Some of these studies require numerical simulations of the refrigerant flow through the valves and inside the cylinder during the compression cycle [2], whereas other studies focus mainly on the dynamics of motion in steady and transient conditions [3]. For instance, a study that included the coupling of fluid-structure dynamics to analyze the dynamics of piston is presented in [4]. Reference [5] shows an analytical model of the coupled dynamic behavior of the piston and crankshaft, with comparisons between a finite bearing model and a short

Manuscript received April 29, 2007; Revised version received Octob. 3, 2007. The authors gratefully acknowledge the support given by the Programme Alþan, the European Union Programme of High Level Scholarships for Latin America, scholarship No. E06D101992CO.

Edgar A. Estupiñan (corresponding author) is with the Mechanical Engineering Department, Technical University of Denmark, Kgs. Lyngby, DK 2800 Denmark. (phone: +45- 4525-5678; fax: +45-4593-1475; e-mail: eep@mek.dtu.dk).

Ilmar F. Santos, is Associate Professor of the Mechanical Engineering Department, Technical University of Denmark, Kgs. Lyngby, DK 2800 Denmark. (e-mail: ifs@mek.dtu.dk).

bearing approach. In the same study, a numerical procedure combining Newton-Raphson method and the successive over relaxation scheme to solve the equations was presented. In the study carried out by Cho and Moon [4], a time-incremental numerical algorithm to solve a finite differences model for the estimation of the oil film pressure is coupled with a finite element model for the computation of the structural deformation of the piston.

Although most of the work done related to modeling of compressors is related to the thermal and fluid dynamic behavior, in this work the main focus and contribution are on the developing of a multibody dynamic model that represents the dynamics of the main mechanical components of hermetic compressors. This model is coupled with a finite element model of the rotor, where the hydrodynamic interaction forces are computed using analytical solutions of Reynolds equation. The elasto-hydrodynamic theory, which takes into account the bearing and housing flexibility, is not considered in this paper, since it is presented only in very special cases.

## II. MATHEMATICAL MODELING

In this section the formulation of representative equations describing the mathematical simulation model for a hermetic compressor is developed. The motion of the piston has been modeled as particle, the motion of the connecting rod and crank as rigid bodies and the shaft is modeled as a flexible body via finite elements. The motion equations for the piston connecting-rod crank system are formulated using the Newton-Euler's method. Fig. 2 shows a sketch indicating the inertial referential frame system XYZ and the main angles of rotation for the moving reference frames.

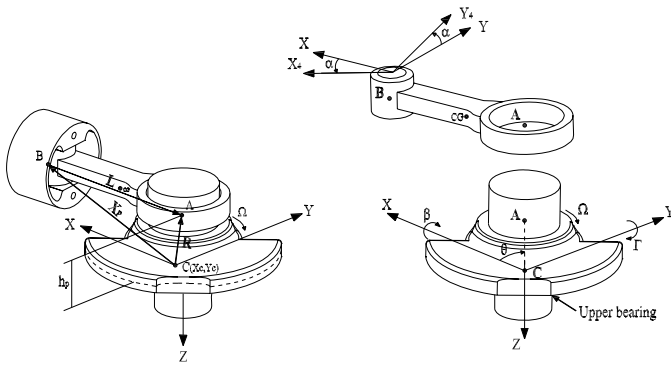


Fig. 2. Piston – connecting rod – crank system. Geometry and reference frames

### A. Reference Frames

One inertial reference frame ( $I_{XYZ}$ ) and four moving reference frames ( $B_1$ ,  $B_2$ ,  $B_3$  and  $B_4$ ) have been defined. The reference frames  $B_1$ ,  $B_2$  and  $B_3$  are attached to the crank to describe the tilting and rotational movement of the crank and the reference frame  $B_4$  is attached to the connecting rod.  $B_1$  ( $X_1Y_1Z_1$ ) is obtained by rotating  $I$  the angle  $\beta$  around  $X$  axis;

$B_2$  ( $X_2Y_2Z_2$ ), is obtained by rotating  $B_1$  the angle  $\Gamma$  around  $Y_1$  axis;  $B_3$  ( $X_3Y_3Z_3$ ), is obtained by rotating  $B_2$  the angle  $\theta$  around  $Z_2$  axis and  $B_4$  ( $X_4Y_4Z_4$ ), is obtained by rotating  $I$  the angle  $\alpha$  around  $Z$  axis.

### B. Constraint Equations

A constraint equation that takes into account lateral displacements and tilting oscillations of the center of the crank is given in (1). A simplified sketch illustrating how the basic elements of the system are connected is shown in Figure 2b.

$${}_I \mathbf{X}_p + {}_I \mathbf{L} = {}_I \mathbf{R} + {}_I \mathbf{C} \quad (1)$$

where:  ${}_I \mathbf{R} = \mathbf{T}_{\beta}^T \cdot \mathbf{T}_{\Gamma}^T \cdot \mathbf{T}_{\theta}^T \cdot {}_{B_3} \mathbf{R}$  ;  ${}_{B_3} \mathbf{R} = \{ r_c \quad 0 \quad -h_p \}^T$

### C. Kinematics

The absolute angular velocity ( $\omega$ ) written with help of  $B_3$ , is given by:

$${}_{B_3} \omega = {}_{B_3} \dot{\beta} + {}_{B_3} \dot{\Gamma} + {}_{B_3} \dot{\theta} \quad (2)$$

where:  ${}_{B_3} \dot{\beta} = \mathbf{T}_{\theta} \cdot \mathbf{T}_{\Gamma} \cdot \mathbf{T}_{\beta} \cdot \dot{\beta}$  ;  ${}_{B_3} \dot{\Gamma} = \mathbf{T}_{\theta} \cdot \mathbf{T}_{\Gamma} \cdot \dot{\Gamma}$  ;  ${}_{B_3} \dot{\theta} = \mathbf{T}_{\theta} \cdot \dot{\theta}$

The velocities and accelerations of the piston ( $\dot{x}_B, \ddot{x}_B$ ) and the connecting rod ( $\dot{\alpha}, \ddot{\alpha}$ ), are obtaining when the constraint equation (1) is differentiated once and twice respectively, obtaining:

$$\begin{bmatrix} 1 & l \sin \alpha \\ 0 & l \cos \alpha \end{bmatrix} \begin{Bmatrix} \dot{x}_B \\ \dot{\alpha} \end{Bmatrix} = \begin{Bmatrix} v_1 \\ v_2 \end{Bmatrix} \quad (3)$$

$$\begin{bmatrix} 1 & l \sin \alpha \\ 0 & l \cos \alpha \end{bmatrix} \begin{Bmatrix} \ddot{x}_B \\ \ddot{\alpha} \end{Bmatrix} = \begin{Bmatrix} a_1 \\ a_2 \end{Bmatrix} \quad (4)$$

where, the variables  $v_1, v_2, a_1, a_2$  are giving in appendix (A).

### D. Equations of Motion

The equations of motion are formulated using Newton-Euler's method [6]. The equations of motion for each body are given in Table I.

The equations of motion for the multibody dynamic model may be written in a matrix form as in (10), where vector  $\bar{\mathbf{f}}$  contains the unknown variables such as: reaction forces, reaction moments and accelerations of the system. This matrix system will be coupled to the equations from the finite element formulation of the crankshaft, which is explained later in section IV.

$$\bar{\mathbf{A}} \cdot \bar{\mathbf{f}} = \bar{\mathbf{c}} \quad (10)$$

TABLE I  
 EQUATIONS OF MOTION

Body	Force Equation	Moment Equation
Crank	$\sum_I \mathbf{F} = m_c \cdot {}_I \bar{\mathbf{a}}_c = {}_I \mathbf{F}_A = m_c \{\ddot{x}_c, \ddot{y}_c\}^T \quad (5)$	$\sum_{B_3} \mathbf{M}_O = {}_{B_3} \mathbf{r} \times {}_{B_3} \mathbf{F}_A + {}_{B_3} \mathbf{T}_m \quad (6)$ $= {}_{B_3} \mathbf{I}_O \frac{d}{dt} ({}_{B_3} \boldsymbol{\omega}) + {}_{B_3} \boldsymbol{\omega} \times ({}_{B_3} \mathbf{I}_O \times {}_{B_3} \boldsymbol{\omega}) + m_c \cdot {}_{B_3} \bar{\mathbf{r}}_{C-cm} \times {}_{B_3} \mathbf{a}_O$ <p>where: <math>{}_{B_3} \mathbf{F}_A = \mathbf{T}_\theta \cdot \mathbf{T}_\Gamma \cdot \mathbf{T}_\beta \cdot {}_I \mathbf{F}_A</math> ; <math>{}_{B_3} \mathbf{T}_m = \{0, 0, T_z\}^T</math> ;  <math>{}_{B_3} \bar{\mathbf{r}}_{C-cm} = \{e_c, 0, 0\}^T</math></p>
Connecting rod	$\sum_I \mathbf{F} = m_{cr} \cdot {}_I \bar{\mathbf{a}}_{cr} = {}_I \mathbf{F}_A + {}_I \mathbf{F}_B \quad (7)$ <p>where:</p> ${}_I \bar{\mathbf{a}}_{cr} = {}_I \mathbf{a}_B + {}_I \dot{\boldsymbol{\alpha}} \times {}_I \dot{\boldsymbol{\alpha}} \times {}_I \bar{\mathbf{r}}_{cr} + {}_I \ddot{\boldsymbol{\alpha}} \times {}_I \bar{\mathbf{r}}_{cr}$ $= \begin{cases} \ddot{x}_B + \bar{r}_{cr} (\dot{\alpha}^2 \cos \alpha + \ddot{\alpha} \sin \alpha) \\ \bar{r}_{cr} (\ddot{\alpha} \cos \alpha - \dot{\alpha}^2 \sin \alpha) \\ 0 \end{cases}$	$\sum_{B_4} \mathbf{M}_B = {}_{B_4} \mathbf{I} \times {}_{B_4} \mathbf{F}_A \quad (8)$ $= {}_{B_4} \mathbf{I}_{cr} \times \frac{d}{dt} ({}_{B_4} \dot{\boldsymbol{\alpha}}) + {}_{B_4} \dot{\boldsymbol{\alpha}} \times ({}_{B_4} \mathbf{I}_{cr} \times {}_{B_4} \dot{\boldsymbol{\alpha}}) + m_{cr} \cdot {}_{B_4} \bar{\mathbf{r}}_{cr} \times {}_{B_4} \mathbf{a}_B$ <p>where: <math>{}_{B_4} \mathbf{F}_A = \mathbf{T}_{\alpha I} \mathbf{F}_A</math> ; <math>{}_{B_4} \mathbf{a}_B = \mathbf{T}_{\alpha I} \mathbf{a}_B</math> ; <math>{}_I \mathbf{a}_B = \{\ddot{x}_B, 0, 0\}^T</math></p>
Piston	$\sum_I \mathbf{F}_B = m_p \cdot {}_I \mathbf{a}_B = {}_I \mathbf{F}_B + {}_I \mathbf{N} + {}_I \mathbf{F}_p \quad (9)$ <p>where: <math>{}_I \mathbf{F}_p = \{P_g \cdot A_p, 0, 0\}^T</math></p>	

where:

$$\bar{\mathbf{f}} = \{f_{B_x}, f_{B_y}, f_{B_z}, N_y, N_z, f_{A_x}, f_{A_y}, f_{A_z}, f_{C_x}, \ddot{\theta}, \ddot{x}_B, \ddot{\alpha}, \ddot{q}_1, \ddot{q}_2, \ddot{q}_3, \ddot{q}_4\}^T$$

and  $\ddot{q}_1, \ddot{q}_2, \ddot{q}_3, \ddot{q}_4$ , correspond to the angular accelerations of the crank center.

#### A. Modeling of the Rotor

The main rotor-shaft of the compressor, which drives the crank-connecting rod-piston system, is modeled as a flexible body via finite elements method [7]. The global equation of motion described in the inertial reference frame is given by:

$$\overline{\mathbf{M}} \cdot \ddot{\mathbf{q}} = \overline{\mathbf{F}} - \overline{\mathbf{D}} \cdot \dot{\mathbf{q}} - \overline{\mathbf{K}} \cdot \mathbf{q} \quad (11)$$

$$\underbrace{\hspace{10em}}_{\bar{\mathbf{f}}}$$

where  $\overline{\mathbf{F}}$ , is the vector that includes the external forces on the rotor such as: preload forces, rotor unbalance forces and the fluid film bearing forces.

### III. FLUID FILM FORCES

The main geometrical relations of a journal bearing are shown in Fig. 3. The governing equation for the pressure distribution of the oil film in dynamically loaded journal bearings may be obtained from the general formulation of Reynolds' equation [8]. The modified Reynolds equation for dynamically loaded journal bearings is given by (12), where,

$\dot{\phi}$  is the rotational speed of the journal center about the bearing center and  $\varepsilon$  is the relative eccentricity. The fluid film thickness may be calculated using:  $h_b = c_b(1 + \varepsilon \cos \varphi)$ , where  $\varphi$  is the angle measured from the location of the maximum film thickness.

$$\frac{\partial}{\partial \varphi} \left( \frac{h_b^3}{\mu} \frac{\partial p}{\partial \varphi} \right) + r_b^2 \frac{\partial}{\partial z} \left( \frac{h_b^3}{\mu} \frac{\partial p}{\partial z} \right) = 12c_b r_b^2 \left[ \frac{\partial \varepsilon}{\partial t} \cos \varphi + \varepsilon \sin \varphi \left( \frac{\partial \phi}{\partial t} - \frac{\Omega}{2} \right) \right] \quad (12)$$

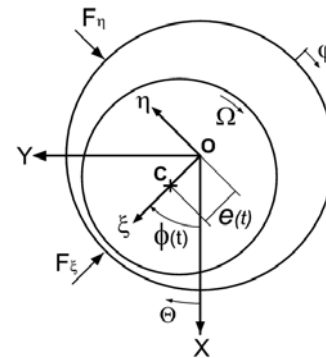


Fig. 3. Journal bearing geometry

With dynamically loaded bearings the eccentricity and attitude angle will vary through the loading cycle. The pressure generated when a journal bearing is dynamically loaded can be determined if the normal squeeze velocity ( $\dot{\varepsilon}$ ) and the rotational velocities ( $\dot{\phi}, \Omega$ ) are known at any eccentricity ratio. Complete solutions of (12) may be obtained

numerically, and solutions for limited cases may be also obtained analytically. In this work analytical solutions for the short-width bearing and infinitely-long-width bearing theories have been used. The short-journal-bearing theory assumes that the variation of pressure is more significant in the axial direction than in the circumferential direction and therefore the first term in (12) can be neglected. In contrast, for an infinitely long-width-journal-bearing, the pressure in the axial direction is assumed to be constant, therefore, in this case, the side-leakage term, i.e., the second term in (12), can be neglected. For each one of these two particular cases, the fluid film pressure distribution can be easily computed, analytically integrating the Reynolds equation and similarly, the journal bearing forces in  $\xi, \eta$  coordinates can be calculated, integrating the pressure distribution analytically obtained. If the pressure is integrated over all the fluid film around the bearing (i.e.,  $0 \leq \varphi \leq 2\pi$ ), this solution is known as a full Sommerfeld solution. However, if the analysis is limited to the convergent film (i.e.,  $0 \leq \varphi \leq \pi$ ), this is known as a half Sommerfeld solution. The analytical expressions used in this paper for the computation of the radial and transversal fluid film forces ( $F_\xi, F_\eta$ ), for a long and a short journal bearing, are giving in [9].

#### IV. NUMERICAL SOLUTION

The equation of motions for each connected body of the multibody system together with the *FEM* model of the shaft and the analytical expressions for the fluid film forces yield to a system of high complexity and non-linearity. The numerical algorithm implemented is shown in Fig. 4. Considering that the system has a "stiff" behavior because of the combination of a rigid body model with a finite element model, a Newmark implicit method combined with a predictor-corrector approach [10], is used in this work. The simulation procedure is summarized in the following main steps:

*Input data and starting values.* In this part the geometrical and physical parameters must be given, such as, physical dimensions, rotational speed, masses, inertias, preloads, initial displacements and initial velocities.

*Pre-processing.* This part includes the generation of structural matrices for the multibody model (**MBD** module) and the matrices of the flexible rotor (**FEM** module). Based on the initial conditions, initial fluid film forces are computed using the **FFF** module.

*Numerical computation.* This part includes the coupling of matrices, the computation of the journal bearing forces at each time step and the numerical solution of the global system. At each time step, new fluid film forces are computed and included in the global matrix system (13) where the equilibrium has to be achieved. In (13), the matrix  $\hat{\mathbf{M}}$  is

formed by the matrix  $\overline{\mathbf{M}}$  of size  $ndof \times ndof$ , coupled to the matrix  $\overline{\mathbf{A}}$  of size  $16 \times 16$  in the degrees of freedom related to the linear and angular accelerations of the crank center node  $(\ddot{q}_1, \ddot{q}_2, \ddot{q}_3, \ddot{q}_4)$ . Thus, the final size of the global mass matrix ( $\hat{\mathbf{M}}$ ) is  $ndof + 12$ . Similarly, in (13) the global right hand side vector,  $\hat{\mathbf{Q}}$ , is formed by coupling the resultant right hand side vector,  $\overline{\mathbf{f}}$ , in (11), to the vector  $\overline{\mathbf{c}}$ , in (10). The iterative equations to solve the global system (13), by using the Newmark implicit method, are given by (14)-(16).

$$\hat{\mathbf{M}} \cdot \{\hat{\mathbf{f}}, \hat{\mathbf{q}}\}^T = \hat{\mathbf{Q}} \quad (13)$$

where:

$$\hat{\mathbf{f}} = \{f_{B_x}, f_{B_y}, f_{B_z}, N_y, N_z, f_{A_x}, f_{A_y}, f_{A_z}, f_{C_z}, \ddot{\theta}, \ddot{x}_B, \ddot{\alpha}\}^T \text{ and}$$

$$\hat{\mathbf{q}} = \{\ddot{q}_1, \ddot{q}_2, \dots, \ddot{q}_{ndof}\}^T.$$

$$\{\hat{\mathbf{f}}_{t_{i+1}}, \hat{\mathbf{q}}_{t_{i+1}}\}^T = \hat{\mathbf{M}}_{t_{i+1}}^{-1} \cdot \hat{\mathbf{Q}}_{t_{i+1}} \quad (14)$$

$$\dot{q}_{t_{i+1}} = \dot{q}_{t_i} + h \left[ (1 - \hat{\gamma}) \ddot{q}_{t_i} + \hat{\gamma} \ddot{q}_{t_{i+1}} \right] \quad (15)$$

$$q_{t_{i+1}} = q_{t_i} + h \dot{q}_{t_i} + \frac{h^2}{2} \left[ (1 - 2\hat{\beta}) \ddot{q}_{t_i} + 2\hat{\beta} \ddot{q}_{t_{i+1}} \right] \quad (16)$$

V. NUMERICAL RESULTS

The main geometrical dimensions and physical properties of the reciprocating compressor used for the numerical simulations are given in Table II. The curve of gas pressure ( $P_g$ ) as function of the crank angle, used for the simulations in this work, is giving in [4] and is shown in Fig. 5. An experimental curve of motor torque for a typical motor of a hermetic compressor is taken from [1] and shown in Fig. 6.

The following results were obtained, using a computer code implemented according to the flow chart of Fig. 4 and using a time step of  $\Delta t = 1e-6$  s to warranty the convergence of the solution.

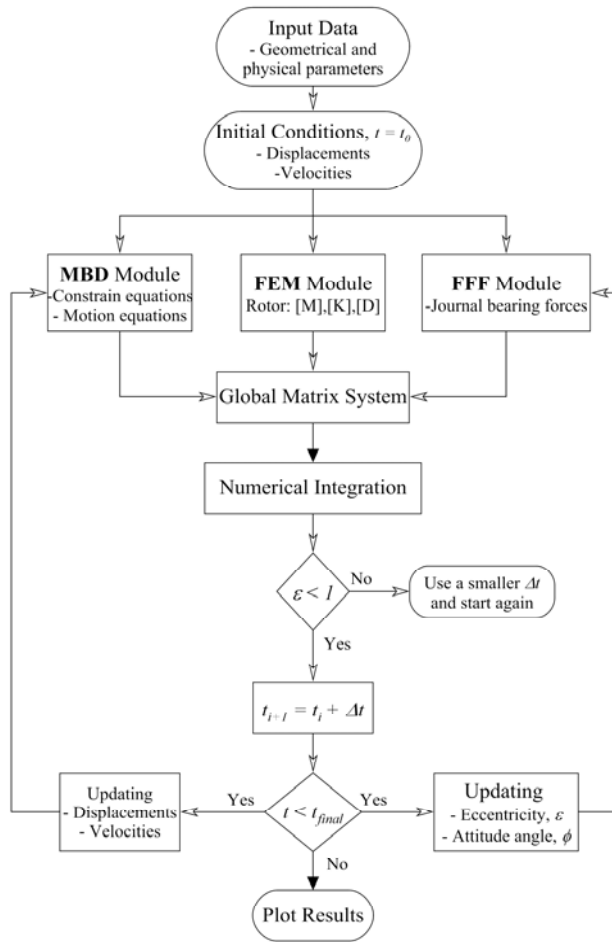


Fig. 4. Flowchart of the numerical computer code

TABLE II. MAIN GEOMETRICAL AND PHYSICAL PARAMETERS

Radius crank-pin center	$r_c = 7.5 \text{ mm}$
Radius of bearings	$r_b = 8 \text{ mm}$
Width of bearings	$l_b = 6 \text{ mm}$
Journal clearance	$c_b = 15 \text{ }\mu\text{m}$
Length of crank pin	$h_p = 10 \text{ mm}$
Distance between bearings	$L = 80 \text{ mm}$
Moments of inertia of motor-rotor	$I_x, I_y = 0.4 \times 10^{-3} \text{ kg.m}^2$ , $I_z = 0.1 \times 10^{-2} \text{ kg.m}^2$
Diameter of piston	$D_p = 23 \text{ mm}$ ( $A_p = 415.5 \text{ mm}^2$ )
Mass of the piston	$m_p = 0.043 \text{ kg}$
Lubricant viscosity	$\mu = 0.005 \text{ Pa.s}$
Angular velocity	$\Omega = 312 \text{ rad/s}$ (2980 rpm)
Crank unbalance	$m_{ub} = 0.05 \text{ kg}$ , $r_{ub} = 5 \text{ mm}$

To compute  $\ddot{q}_{i+1}$ , the load vector  $\hat{Q}_{i+1}$  must be estimated previously, which implies to calculate the vector of journal bearing forces  ${}_b Q_{i+1}$ , which depends on the positions and velocities at the time  $t_{i+1}$ . Therefore, initial values for  $\dot{q}_{i+1}^0$  and  $q_{i+1}^0$  are predicted by using the Heun's explicit method. Then,  $\ddot{q}_{i+1}^1$  can be initially estimated by using (14) and then,  $\dot{q}_{i+1}^1$  and  $q_{i+1}^1$  can be calculated using (15) and (16) respectively. With these new estimated values, the journal bearing forces are updated and using again (14) a new estimation of  $\ddot{q}_{i+1}^2$  can be obtained, and so on until the difference of two consecutive values is smaller than the prescribed tolerance given. Additionally, by using the explicit Euler method, the crank angle  $\theta_i$  and the instantaneous angular velocity  $\dot{\theta}_i$  are estimated at each time step.

*Post-processing.* This part includes the generation of plots of journal bearing orbits, journal bearing forces, maximum oil film pressure, minimum fluid film thickness and reaction forces as a function of the instantaneous crank angle.

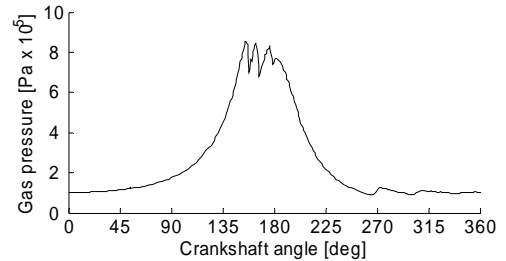


Figure 5. Curve of the gas pressure ( $P_g$ ) as a function of the crankshaft angle

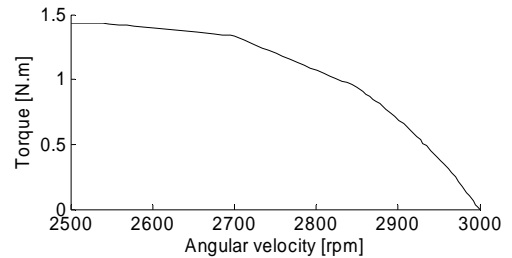


Fig. 6. Curve of the motor torque ( $T_m$ ) as a function of the angular velocity.

Fig. 7 shows the journal bearing forces for the upper and

lower bearing. It can be observed from this figure that the maximum forces are found when the piston is close to the top dead center (i.e., when the pressure inside the cylinder is maximal). It can be also noticed a transient oscillation, damped a few cycles, and which is more evident for the lower bearing due to the lower values of the bearing forces.

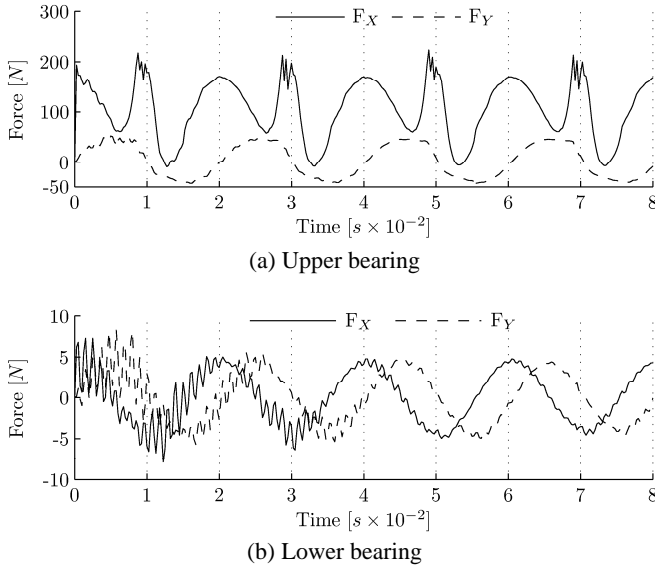


Fig. 7. Journal bearing forces

The minimum fluid film thickness is plotted in Fig. 8, which shows that the lowest values of oil film thickness are found during the compression cycle, approximately 65° before the piston reaches the top dead center (i.e., when  $\theta \approx 115^\circ, \theta \approx 475^\circ, \theta \approx 835^\circ, \dots$ ).

The maximum pressure is shown in Fig. 9, where it can be seen that the highest pressure values are found in the intervals between the times when the minimum fluid film thickness is reached at each cycle and the top dead centre position ( $\theta \approx 180^\circ, \theta \approx 540^\circ, \theta \approx 900^\circ, \dots$ ). This plot, shows the maximum pressure computed for two different lengths ( $h_p = 0$  and  $h_p = 10\text{mm}$ ) and it is observed a transient oscillation when the length of the crank pin is used, which comes from higher vibration modes of the flexible rotor influenced by the tilting oscillations of the crank.

Fig. 10 compares the minimum film thickness using a length of the crank pin of  $h_p = 10\text{mm}$  and  $h_p = 0$ . It can be observed in this figure that the difference between the lowest values of minimum film thickness could be as high as 18% (e.g., at  $\theta \approx 1180^\circ$ ). Therefore, the length of the crank pin is a parameter that should be included in the calculations, particularly when the tilting oscillations are considered in the model.

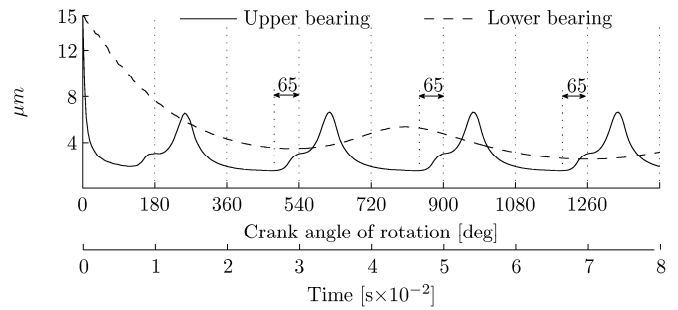


Fig. 8. Minimum fluid film thickness for the upper and lower bearing

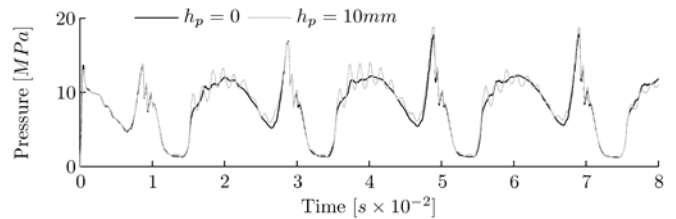


Fig. 9. Maximum fluid film pressure in upper journal bearing

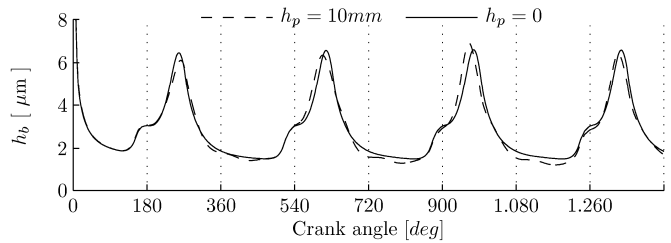


Fig. 10. Influence of the crank pin length ( $h_p$ ) in the computation of the minimum fluid film thickness

Fig. 11 shows orbits of the upper bearing obtained for cases with different amount of unbalance of the crank. It can be seen in this figure that the orbit of the journal tends to be bigger when the amount of unbalance increases, but the stationary position around which the orbit is generated does not change, which is expected because no additional static forces have been added. The orbits obtained has a similar shape compared to orbits predicted theoretically in several studies related to the analysis of main journal bearings of internal combustion engines [11], [12].

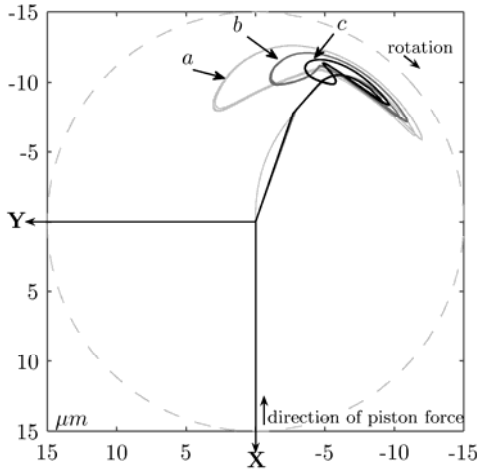


Fig. 11. Orbits of upper journal bearing, varying the amount of crank unbalance ( $m_{ub}$ ). (a)  $m_{ub} = 0.05\text{kg}$ , (b)  $m_{ub} = 0.05\text{kg}$ , (c)  $m_{ub} = 0\text{kg}$ .

## VI. CONCLUSION

In the model of the compressor developed, the lateral and tilting vibration of the crank have been included. Therefore and considering that the oil film thickness is only a few micrometers thick, more precise estimations of the journal bearing forces and minimum film thickness are obtained. The simulations were carried out for a short bearing, with a width to radius ratio equal to 0.75, therefore the use of the short bearing approach was preferred for this study. The maximum forces and the minimum fluid film thickness are obtained when the piston is close to the top dead centre.

The influence of the amount of unbalance was studied and it was found that, although it influences the orbit of motion of the journal, the journal forces and the minimum film thickness do not change significantly. The consideration that the reaction forces coming from the crank pin are out of the plane of the centre of mass of the crank, was taking into account including in the equations the crank pin length. The results showed differences up to 20% for the minimum film thickness and 5% for the maximum pressure when the length of the crank was included in the equations, due mainly to the increase in the tilting oscillations of the crank.

## APPENDIX

### (A). KINEMATIC VARIABLES

$$v_1 = -r_c(\dot{\Gamma}s\Gamma c\theta + \dot{\theta}c\Gamma s\theta) - h_p\dot{\Gamma}c\Gamma + \dot{x}_c$$

$$v_2 = r_c\dot{\beta}(c\beta s\Gamma c\theta - s\beta s\theta) + r_c\dot{\theta}(c\beta c\theta - s\beta s\Gamma s\theta) + \dot{\Gamma}(r_c s\beta c\Gamma c\theta - h_p s\beta s\Gamma) + \dot{\beta}h_p c\beta c\Gamma + \dot{y}_c$$

$$a_1 = -r_c\ddot{\Gamma}s\Gamma c\theta + \dot{\Gamma}^2(h_p s\Gamma - r_c c\Gamma c\theta) + 2r_c\dot{\theta}\dot{\Gamma}s\Gamma s\theta - r_c\dot{\theta}_2 c\Gamma c\theta - h_p\ddot{\Gamma}c\Gamma - r_c\ddot{\theta}c\Gamma s\theta - l\dot{\alpha}^2 c\alpha + \ddot{x}_c$$

$$a_2 = -r_c\dot{\theta}^2(c\beta s\theta + s\beta s\Gamma c\theta) - \dot{\beta}^2(r_c c\beta s\theta + r_c s\beta s\Gamma c\theta + h_p s\beta c\Gamma) - \dot{\Gamma}^2(r_c s\beta s\Gamma c\theta + h_p s\beta c\Gamma) + \dot{\beta}(h_p c\beta c\Gamma - r_c s\beta s\theta + r_c c\beta s\Gamma c\theta) + \ddot{\Gamma}(r_c s\beta c\Gamma c\theta - h_p s\beta s\Gamma) - 2r_c\dot{\theta}\dot{\beta}(s\beta c\theta + c\beta s\Gamma s\theta) + 2\dot{\beta}\dot{\Gamma}(r_c c\beta c\Gamma c\theta - h_p c\beta s\Gamma) - 2r_c\dot{\theta}\dot{\Gamma}s\beta c\Gamma s\theta + r_c\ddot{\theta}(c\beta c\theta - s\beta s\Gamma s\theta) + l\dot{\alpha}^2 s\alpha + \ddot{y}_c$$

where:  $s\theta = \sin \theta$ ;  $c\theta = \cos \theta$ ;  $s\alpha = \sin \alpha$ ;  $c\alpha = \cos \alpha$ ;  $s\beta = \sin \beta$ ;  $c\beta = \cos \beta$ ;  $s\Gamma = \sin \Gamma$ ;  $c\Gamma = \cos \Gamma$ .

### (B). NOMENCLATURE

Symbol	Quantity	Units
$A_p$	transversal area of the piston	$\text{m}^2$
$c_b$	radial clearance of bearing	m
$F_{\xi}, F_{\eta}$	radial and transversal fluid film forces	
$h_b$	oil film thickness	m
$h_p$	length of crank pin	m
$l$	length of the connecting rod	m
$l_b$	width of bearing	m
$m$	mass	kg
$ndof$	number of degrees of freedom	
$P_g$	pressure of gas inside the cylinder	Pa
$rpm$	revolutions per minute	
$r_b$	radio of bearing	m
$r_c$	radius crank-pin center	m
$\mathbf{T}_i$	transformation matrix in the $i$ -th coordinate	
$T_z$	motor shaft torque	N.m
Greek symbols		
$\Omega$	rotational speed of the rotor and	Rpm
$\dot{\theta}$	rotational speed of the rotor	rad/s
$\theta$	rotation angle of the crank	rad
$\alpha$	rotation angle of the connecting rod	rad
$\beta$	rotation angle around X-X axis	rad
$\Gamma$	rotation angle around Y-Y axis	rad
$\mu$	viscosity oil film	Pa.s
$\varepsilon$	eccentricity ratio	
$\phi$	attitude angle	rad
$\xi, \eta$	radial and transversal directions	
Subscripts		
$b$	bearing	
$B_i$	$i$ -th mobile reference frame	
$c$	crank	
$cr$	connecting rod	
$p$	Piston	
$ub$	Unbalance	

## REFERENCES

- [1] J. Rigola, "Numerical simulation and experimental validation of hermetic reciprocating compressors", PhD dissertation, Universidad Politécnica de Cataluña, Barcelona, Spain, 2002.
- [2] G. Longo and A. Gasparella, "Unsteady state analysis of the compression cycle of a hermetic reciprocating compressor", *International Journal of Refrigeration*, vol. 26, no. 6, pp. 681-689, 2003.
- [3] R. Dufour, J. Der Hagopian and M. Lalanne, "Transient and steady state dynamic behaviour of single cylinder compressors: Prediction and experiments", *Journal of Sound and Vibration*, vol. 181, no. 1, pp. 23-41, 1995.
- [4] J. R. Cho and S. J. Moon, "A numerical analysis of the interaction between the piston oil film and the component deformation in a reciprocating compressor", *Tribology International*, vol. 38 no. 5, pp. 459-468, 2005.
- [5] T. J. Kim and J. S. Han, "Comparison of the dynamic behavior and lubrication characteristics of a reciprocating compressor crankshaft in both finite and short bearing models", *Tribology Transactions*, vol. 47, no. 1, pp. 61-69, 2004.
- [6] I. F. Santos, *Dinâmica de Sistemas Mecânicos*, (in Portuguese). Makron Books, Sao Paulo, Brazil, 2001.
- [7] H. D. Nelson, "A finite rotating shaft element using Timoshenko beam theory", *Journal of Mechanical Design, Transactions of the ASME*, vol. 102, no. 4, pp. 793-803, 1980.
- [8] B. J. Hamrock, *Fundamental of Fluid Film Lubrication*, NASA Reference Publication, USA, 1991.
- [9] J. Frêne, D. Nicolas, B. Degueurce, D. Berthe and M. Godet, *Lubrification Hydrodynamique*, Editions Eyrolles, Paris, 1990.
- [10] J. Garcia de Jalon and E. Bayo, *Kinematic and Dynamic Simulation of Multibody Systems. The Real-Time Challenge*, Springer-Verlag, New-York, 1994.
- [11] R. Pal, R. Sinhasan and D. Singh, "Analysis of a big-end bearing - a finite element approach", *Wear*, vol. 121, no. 1, pp. 117-120, 1988.
- [12] G. S. Ritchie, "The prediction of journal loci in dynamically loaded internal combustion engine bearings", *Wear*, vol. 35, no. 2, pp. 291-297, 1975.